HHS Public Access

Author manuscript

Sci Transl Med. Author manuscript; available in PMC 2018 April 05.

Published in final edited form as:

Sci Transl Med. 2017 April 05; 9(384): . doi:10.1126/scitranslmed.aaf4696.

Type I collagen-targeted PET probe for pulmonary fibrosis detection and staging in preclinical models

Pauline Désogère[1,†], **Luis F. Tapias**[2,†], **Lida P. Hariri**[3,4], **Nicholas J. Rotile**[1], **Tyson A. Rietz**[1,‡], **Clemens K. Probst**[3], **Francesco Blasi**[1,§], **Helen Day**[1,♯], **Mari Mino-Kenudson**[4], **Paul Weinreb**[6], **Shelia M. Violette**[6], **Bryan C. Fuchs**[5], **Andrew M. Tager**[3], **Michael Lanuti**[2,*], and **Peter Caravan**[1,*]

[1]The Athinoula A. Martinos Center for Biomedical Imaging, Department of Radiology, Massachusetts General Hospital and Harvard Medical School, Charlestown, Massachusetts, 02129

[2]Division of Thoracic Surgery, Massachusetts General Hospital and Harvard Medical School, Boston, Massachusetts, 02114

[3]Division of Pulmonary and Critical Care Medicine, Massachusetts General Hospital and Harvard Medical School, Boston, Massachusetts, 02114

[4]Department of Pathology, Massachusetts General Hospital and Harvard Medical School, Boston, Massachusetts, 02114

[5]Division of Surgical Oncology, Massachusetts General Hospital and Harvard Medical School, Boston, Massachusetts, 02114

[6]Biogen, Cambridge, Massachusetts, 02142

Abstract

Pulmonary fibrosis is a scarring of the lungs that can arise from radiation injury, drug toxicity, environmental or genetic causes, and for unknown reasons [idiopathic pulmonary fibrosis (IPF)]. Overexpression of collagen is a hallmark of organ fibrosis. Here, we describe a peptide-based PET probe (^{68}Ga-CBP8) that targets collagen type I. We evaluated ^{68}Ga-CBP8 in vivo in the bleomycin-induced mouse model of pulmonary fibrosis. ^{68}Ga-CBP8 showed high specificity for

*Corresponding authors: caravan@nmr.mgh.harvard.edu (P.C.), mlanuti@mgh.harvard.edu (M.L.).
†These authors contributed equally to this work.
†Present address: School of medicine, Vanderbilt University, Nashville, Tennessee.
§Present address: Center of excellence for preclinical imaging, Department of molecular biotechnology and health sciences, University of Turin, Turin, Italy.
♯Present address: College of the Environment and Life Sciences, University of Rhode Island, Kingston, Rhode Island.

Author contributions: P.C. initially conceptualized this project and supervised the entire project. P.D., L.F.T., M.L., A.M.T., L.H. and P.C. conceived the experiments. P.D. developed the synthesis and synthesized the radioactive probes. P.D., L.F.T, N.R., T.A.R., C.K.P., F.B. and H.D. performed the animal experiments. P.D., L.F.T., B.F. and N.R. analyzed the data. P.W. provided the antibodies. M.M.K., B.F. and L.H. analyzed histological data. L.H. enabled the experiment with human tissues. P.D. wrote the manuscript draft, which was then further refined by P.C. All other authors reviewed and edited the intermediate and final versions of the manuscript.

Competing interest: P.C. has equity in Collagen Medical, the company, which holds the patent rights to the peptides used in these probes. S.V. and P.W. are employees of Biogen. A patent has been filled by P.C. and P.D. regarding collagen-binding PET tracer preparation and imaging.

Data and material availability: These patents do not restrict the research or non-commercial use of the probe technique. The probe can be obtained using the synthetic procedures described in the Supplemental Materials.

pulmonary fibrosis and high target:background ratios in diseased animals. The lung PET signal and lung ^{68}Ga-CBP8 uptake (quantified ex vivo) correlated linearly (r^2=0.80) with the amount of lung collagen in mice with fibrosis. We further demonstrated that the ^{68}Ga-CBP8 probe could be used to monitor response to treatment in a second mouse model of pulmonary fibrosis associated with vascular leak. Ex vivo analysis of lung tissue from patients with IPF supported the animal findings. These studies indicate that ^{68}Ga-CBP8 is a promising candidate for non-invasive imaging of human pulmonary fibrosis.

Introduction

Idiopathic pulmonary fibrosis is a specific form of progressive, fibrosing interstitial pneumonia of unknown etiology that primarily affects older adults. In the majority of cases, it is a relentlessly progressive disease that results in dyspnea and functional decline until death (1,2). Currently, there is no treatment able to reverse fibrosis in this disease (3).

Despite efforts to establish precise, universally acknowledged diagnosis criteria for IPF, its ascertainment remains a challenge—although high-resolution computed tomography (HRCT) scanning can aid diagnosis of the disease (4). Patients with suspected IPF that show atypical features on HRCT images usually require a surgical lung biopsy to confirm the diagnosis (5, 6); however, many of these patients have physiological impairments and comorbidities that make biopsy a risky procedure.

These challenges highlight the need for the development and validation of diagnostic and prognostic markers specific to IPF to guide treatment decisions. The ability to recognize fibrosis non-invasively, for example, with innovative molecular imaging techniques, could substantially improve management of patients with fibrotic lung disease. In recent years, collagen degradation markers (7), activated macrophages (8, 9), fibroblasts (10, 11), integrins $\alpha_v\beta_6$ (12, 15) and $\alpha_v\beta_1$ (16) have been studied as diagnostic and prognostic markers. Pulmonary ^{18}F-FDG uptake has also been reported to be a predictor of global health score and lung physiology in patients with IPF (17–19); ^{18}F-FDG, however, lacks specificity for IPF.

We set out to develop an approach based on direct molecular imaging of type I collagen as a noninvasive means of detecting, as well as staging, pulmonary fibrosis. Fibrosis, regardless of its cause or location, is characterized by excess deposition of collagens, primarily type I collagen, and other extracellular matrix proteins in the parenchyma (20). Indeed, histological proof of fibrosis is predicated on collagen staining. We previously described a 16 amino acid disulfide-bridged cyclic peptide that was identified via phage display and that recognized and bound to type I human collagen. This peptide was functionalized with 3 gadolinium diethylenetriaminepentaacetate (DTPA) chelates to provide magnetic resonance (MR) signal enhancement, and the resulting probe (EP-3533) showed excellent ability to detect and stage disease in preclinical models of cardiac (21–22), hepatic (23–25), and pulmonary fibrosis (26).

We have next sought to develop an analogous PET probe. PET is a quantitative modality that provides higher spatial resolution than other nuclear imaging techniques in humans and that

could be used to quantify pulmonary fibrosis. PET is an accepted method that is already frequently used for investigating lung pathology. Equally important is the growing installed base of PET-CT and PET-MR systems. In the absence of lung architectural distortion (which may not be present early in fibrotic lung diseases), fibrosis may be indistinguishable by HRCT from other pathological processes that attenuate X-ray signals, such as inflammation. By fusing collagen-specific PET with HRCT, however, we hoped to be able determine whether specific opacities and patterns identified by HRCT are the result of fibrosing disease (27). In addition, the development of PET molecular imaging probes offers a shorter and more economical path to clinical translation than do MRI probes because the low, microgram mass dose required for PET allows for an abbreviated preclinical safety and toxicology package to be submitted to regulators in order to initiate human studies.

Here, we describe a peptide-based, collagen-targeted PET probe ^{68}Ga-CBP8 and demonstrate its ability to detect and quantify pulmonary fibrosis in two mouse models of disease as well as show its capacity to monitor therapeutic responses. We also evaluated the capacity of the probe to detect fibrosis in lung tissue samples from an IPF patient.

Results

Synthesis, in vitro characterization and pharmacokinetics of ^{68}Ga-CBP8 and ^{68}Ga-CBP12

We synthesized a type I collagen-targeted probe, ^{68}Ga-CBP8, and an inactive negative control probe, ^{68}Ga-CBP12. ^{68}Ga-CBP8 and ^{68}Ga-CBP12 are isomers that differ only in the chirality of the cysteine at the 13th amino acid position from the C-terminus (Fig. S1). The peptide precursors of both probes were conjugated to tris(tert-butyl) ester protected 1,4,7-triazacyclononane,1-glutaric acid-4,7-acetic acid (NODAGA) chelators. We then deprotected the chelating carboxylate groups and purified the peptide conjugates. Radiolabeling was performed under standard conditions, was complete in 5 minutes, and gave high radiochemical yields without the need for HPLC purification (Fig. S2). Specific activities ranged from 324 to 462 GBq/μmol. We estimated type I collagen affinity by incubating increasing concentrations of non-radioactive Ga-probes with either type I rat or type I human collagen (21). The K_d for Ga-CBP8 binding to type I human collagen was 2.1±0.1 μM and 4.6±0.5 μM for rat collagen, while the control compound Ga-CBP12 showed weaker binding to human (K_d = 42±5 μM) and rat (K_d = 50±10 μM) collagens (Fig. S3, S4).

Mice were injected intravenously with approximately 3.7 MBq of either ^{68}Ga-CBP8 or ^{68}Ga-CBP12, and the change in the decay-corrected signal in the heart was measured by PET as a function of time. Both probes showed similar biexponential clearance, and we estimated similar blood half-lives from fits to the data (32.9 ± 4.5 min for ^{68}Ga-CBP8 and 30.4 ± 3.0 min for ^{68}Ga-CBP12; p=ns, n=5 for each probe). Urine was collected at 150 min after probe administration and injected onto an analytical HPLC column, and the results were compared with standards of pure probe. Both probes were > 90% intact in urine, indicating that the probes are highly stable in vivo (Fig S5).

^{68}Ga-CBP8 specifically binds collagen in the bleomycin mouse model of pulmonary fibrosis

A single transtracheal instillation of bleomycin (BM) (2.5 U/kg) results in histopathology consistent with pulmonary fibrosis. Two weeks after instillation, all of the BM-injured mice had histopathological findings of substantial pulmonary fibrosis, including excessive interstitial deposition of collagen as demonstrated by Sirius Red staining, and destruction of lung architecture; sham animals, which received transtracheal saline, showed no signs of pulmonary disease (Fig. 1A). The BM-injured lungs exhibited a lymphoplasmacytic infiltrate along with excessive collagen deposition as visualized with Sirius Red in the areas of fibrosis, with a predominant subpleural and peribronchial distribution. Lungs from sham animals had preserved alveolar architecture, with no excess collagen deposition or alveolar infiltration.

As expected, disease progressed in a stepwise fashion as determined by histological Ashcroft scoring of lung fibrosis (28). Seven days after instillation of BM, most animals had moderate fibrous thickening of alveolar or bronchiolar walls without damage to lung architecture (Ashcroft score of 2.3 ± 0.3; range 2–3, Fig. 1B). Disease progressed with formation of fibrous bands, small fibrous masses, or large fibrous areas with definite damage to lung structure (Ashcroft score of 5.4 ± 0.4; range 4–7 at day 14). The amount of lung tissue affected by the disease (measured with Sirius Red staining) also increased with time: 12% of the area of tissue sections from the right lung of BM-injured mice were affected by disease at day 7, while this increased to 24% at day 14 (Fig. 1C). Sham animals exhibited histologically normal lung tissue sections. Consistently, collagen deposition (as determined by analysis of hydroxyproline (29) content in the left lung) increased progressively with time (Fig. 1D).

To determine whether the ^{68}Ga-CBP8 signal was an accurate reflection of disease progression, we compared mice injured with BM at day 7 and day 14 after instillation. Ex vivo measurement of probe uptake into the lung increased with disease progression in the BM-injured mice (0.028 ± 0.005 percent injected dose per lung (% ID/lung) at day 7; 0.066 ± 0.008 % ID/lung at day 14) (Fig. 1E and Fig. 1F.). Additionally, there was a strong correlation between probe uptake in the lung and lung hydroxyproline content ($r^2 = 0.80$, $p<0.0001$) (Fig. 1G).

To demonstrate the specificity of ^{68}Ga-CBP8, we compared its uptake into lung with that of the isomer ^{68}Ga-CBP12 in which one of the cysteine amino acids was changed from L- to D-chirality. ^{68}Ga-CBP8 accumulated specifically in fibrotic lungs of BM-treated mice but not in the healthy lungs of control mice, whereas ^{68}Ga-CBP12 was not preferentially taken up into lungs of BM-treated mice compared to controls (Fig. 2A). There were no significant differences in hydroxyproline content between the BM-treated mice that received ^{68}Ga-CBP8 and those that received ^{68}Ga-CBP12 (Fig. 2B). The control probe ^{68}Ga-CBP12 showed no preferential uptake in the lungs of BM-injured mice compared to control mice as determined by ex vivo and PET data analysis (Fig. 2C and D). The distribution of ^{68}Ga-CBP12 in other organs was similar to that of ^{68}Ga-CBP8 (Fig. 2E). These results show the in

vivo specificity of ^{68}Ga-CBP8 for type I collagen, which allows the non-invasive detection and monitoring of progression of pulmonary fibrosis in the BM-treated mouse model.

^{68}Ga-CBP8 detects and stages disease in a mouse model of pulmonary fibrosis associated with enhanced vascular permeability

IPF is thought to result when a lung-injuring environmental stimulus is experienced by a person with a genetic predisposition to pulmonary fibrosis. In the context of such a genetic predisposition, fibrosis is thought to result from aberrant or exaggerated wound healing responses to a relatively common and/or mild lung injury, which would be well tolerated and repaired without fibrosis by most people (30, 31). A growing number of mouse models are trying to capture this important “gene-by-environment” nature of pulmonary fibrogenesis (32). We used a low dose bleomycin vascular leak (LDBVL) model that combines the S1P receptor functional antagonist fingolimod (FTY720) to disrupt endothelial barrier function with low-dose BM to induce mild lung injury (33). Sustained exposure to FTY720 causes increased vascular leak and intra-alveolar coagulation after lung injury, which also leads to an exaggerated fibrotic response to a low dose of BM challenge (33).

One group of mice (LDBVL) was treated with a low dose of BM and the vascular leak agent FTY720 (n=9). A second group (LDB) (n=4) received a low dose of BM, and the third (FTY) (n=6) received the vascular leak agent only. FTY720 was administered intraperitoneally to the mice at 1 mg/kg three times a week (Fig. 3A). The three groups were imaged at day 14 after BM or vehicle instillation. After imaging the mice were euthanized and the right lung taken for histopathology analysis and the left lung taken for biochemical analysis. The LDBVL mice showed an average fibrosis score of 6 (± 0.2; range 4–7), the LDB mice showed an average fibrosis score of 1.5 (± 0.9; range 0–3), whereas all mice given FTY showed a score of 0 (Fig. 3B). Less than 1% of the total area of tissue sections from the right lung was affected by disease in LDB animals (measured by Sirius Red staining), while 15% of the total area was affected by disease in the LDBVL group (Fig. 3C). There was no area affected by disease in the right lungs of the FTY animals upon histological examination. Fig. 3D shows twice as much hydroxyproline in the left lung of LDBVL animals compared with LDB and FTY mice (116.9 ± 4.0 μg for LDBVL, 59.1 ± 4.4 μg for LDB, 49.2 ± 2.6 μg for FTY, $p<0.0001$). There was no significant difference in hydroxyproline content in the left lung between LDB and FTY animals ($p=0.4057$).

Consistently, PET quantification showed a significantly higher signal in lungs of LDBVL mice (2.9 ± 0.2 %ID/cc) compared to lungs of FTY (1.5 ± 0.1 %ID/cc, $p<0.0001$) and compared to LDB animals (1.7 ± 0.1 %ID/cc, $p<0.0001$, Fig. 3E). There was no significant difference in lung signal measured by PET images analysis between the FTY group and the LDB group ($p=0.9156$). Ex vivo quantification of ^{68}Ga-CBP8 uptake revealed five times more uptake in the LDBVL group than in the FTY group ($p<0.0001$) and three times more in the LDBVL group compared to the LDB group ($p<0.0001$) (Fig. 3F). The difference in lung uptake between the LDB and the FTY groups was not statistically significant ($p=0.8202$). Hydroxyproline content was strongly correlated with %ID/cc ($r^2=0.84$, $p<0.0001$) (Fig. 3G), and %ID/lung ($r^2=0.93$, $p<0.0001$) (Fig. 3H). These results

demonstrate the in vivo specificity of ^{68}Ga-CBP8 for detection of excess collagen deposition in a second model of pulmonary fibrosis.

In a separate group of LDBVL mice, we performed a test-retest study. Reproducibility was evaluated in seven LDBVL mice by scanning each mouse twice, with an interval of 24h between scans, 13 days after BM instillation. Paired t-tests revealed no statistically significant difference between the values of %ID/cc between test and retest for both lung and muscle regions of interest (p=0.8262). Reproducibility was calculated by using the %ID/cc of the first scanning segment in lung or muscle, as 100×[%ID/cc(test)−%ID/cc(retest)]/%ID/cc(test). Within subject test-retest variability was <12% in the lungs and <7% in muscle. The intra-class correlation coefficient, which is a measure of the reliability of within-subject data relative to between-subject data, was 0.93 for lung analysis and 0.99 for muscle analysis (34). Reproducible measurements in mouse lungs are challenging to obtain because of the variation in lung density within individual mice. Breathing rate and position of the subject in the scanner are also factors influencing reproducible measurement in the lungs (35). Nevertheless, our test-retest experiment illustrates that quantitation of fibrosis with ^{68}Ga-CBP12 can yield reproducible results.

^{68}Ga-CBP8 PET allows monitoring of the response to anti-fibrotic therapy in mice

We monitored the anti-fibrotic effects of 3G9, a murine antibody targeted to integrin $\alpha_v\beta_6$, with ^{68}Ga-CBP8 PET. The humanized version of 3G9 is STX-100 (Biogen), has successfully completed Phase 1 clinical testing and is now under investigation in a Phase 2 clinical trial of IPF (Clinicaltrials.gov Identifier: NCT01371305). Integrin $\alpha_v\beta_6$ is a key activator of TGF-β signaling in the lung (12, 13), and specific targeting of $\alpha_v\beta_6$ with 3G9 can partially prevent pulmonary fibrosis in mice without systemic disruption of other homeostatic roles of TGF-β (36, 37).

Mice injured with a low dose of bleomycin and the vascular leak agent were treated with the anti-$\alpha_v\beta_6$ antibody 3G9 (LDBVL+3G9 group) or the irrelevant isotypic antibody 1E6 (LDBVL+1E6 group) (37). In this study, a control group of mice received the 3G9 antibody only (3G9 group). FTY720 was administered intraperitoneally to the mice at 1 mg/kg three times a week starting on day 0. Both 3G9 (anti-$\alpha_v\beta_6$ antibody) and the control antibody 1E6 were injected into mice intraperitoneally three times per week at a concentration of 1 mg/kg starting on day 0. PET-CT imaging, biodistribution and hydroxyproline analysis were performed on LDBVL+3G9, LDBVL+1E6 and 3G9 mice 14 days after the initiation of administration of the different compounds (n=11, n=11 and n=5), and data were compared to data for the LDBVL group (n=9) shown in Fig 3.

Treatment with the therapeutic antibody 3G9 reduced pulmonary fibrosis in LDBVL group as assessed by histology (Fig. 4B) and by hydroxyproline quantification (Fig. 4C). LDBVL mice showed an average fibrosis score of 6 (± 0.2; range 4–7), while LDBVL+3G9 mice had an average score of 4 (± 0.4; range 1–6), (LDBVL+1E6) mice showed an average fibrosis score of 6 (± 0.3; range 5–7), and mice treated with 3G9 alone had histologically normal lungs with a score of 0. Fourteen percent of the total area of right lung tissue sections was affected by disease in LDBVL mice, while this value was 7% for the LDBVL+3G9 group, and 18% for LDBVL+1E6 animals. There was no lung area affected by disease in 3G9-

treated animals. Hydroxyproline analysis of the left lung showed significantly lower values in lungs of LDBVL+3G9 mice compared to the LDBVL and LDBVL+1E6 mice (83.8 ± 2.7 μg per left lung for LDBVL+3G9 mice, 116.5 ± 4.9 μg for LDBVL mice, 108.9 ± 3.5 μg for LDBVL+1E6 mice). There were no significant differences in hydroxyproline content between LDBVL+3G9 and 3G9-treated mice, or between LDBVL and LDBVL+1E6 mice.

Similar effects of 3G9 treatment were also seen by lung PET imaging, where the lung PET signal was similar to what was seen in control mice and significantly lower than what was observed in the fibrotic group (Fig. 4A). Quantification of the ^{68}Ga-CBP8 PET signal showed 1.5 times higher lung uptake in the LDBVL animals that received the irrelevant antibody (fibrotic mice, LDBVL+1E6, 3.0 ± 0.2 %ID/cc) than in mice of the LDBVL group treated with the anti-$\alpha_v\beta_6$ antibody (LDBVL+3G9, 1.9 ± 0.2 %ID/cc, p=0.0017) (Fig. 4D). Organ uptake measured by ex vivo analysis was not significantly different among groups, except for the lungs where there was three times more uptake in the LDBVL+1E6 group than in the LDBVL+3G9 group (p=0.0004) and six times higher uptake in the LDBVL+1E6 group than in the 3G9-treated group (p<0.0001) (Fig. 4E). Lung uptake of ^{68}Ga-CBP8 was not statistically different between the LDBVL+3G9 group and the 3G9-treated group (p=0.4524). These results illustrate that ^{68}Ga-CBP8 enables non-invasive monitoring of in vivo responses to therapeutic interventions in animals affected by pulmonary fibrosis.

Probe ^{68}Ga-CBP8 allows monitoring of collagen content in human IPF lung samples

To determine whether our findings could be translated to human tissues, we evaluated the binding of the probe ^{68}Ga-CBP8 to fresh human lung tissues from three IPF patients undergoing pneumonectomy prior to lung transplantation. Lung tissues were collected fresh within one hour of resection. Three sampling areas were defined in the lung of the patient: the superior upper lobe (S1), the lateral upper lobe (S2) and the lower lobe (S3) and chunks of tissues were sampled in these three areas. We incubated samples from S1, S2 and S3 (70 to 100 mg) with ^{68}Ga-CBP8 for 2 hours (n=5 per area) and quantified the probe uptake. Once ^{68}Ga-CBP8 radioactivity had decayed, we incubated the samples with ^{68}Ga-CBP12 for 2 hours and quantified ^{68}Ga-CBP12 uptake. The uptake of ^{68}Ga-CBP8 in human lung samples showed differences in collagen concentration among lobes in the three IPF patients and heterogeneity of disease progression among patients (Fig 5A). ^{68}Ga-CBP12 uptake was significantly lower than ^{68}Ga-CBP8 in all samples. We performed histological analyses on samples just adjacent to those used for probe incubation (Fig. 5B). Uptake of ^{68}Ga-CBP8 in IPF human lung tissue samples increased linearly with increasing fibrosis as measured by Sirius Red quantification of the area affected by disease (r^2=0.94, p<0.0001, (Fig. 5B). The ^{68}Ga-CBP12 signal did not change with collagen concentration in IPF human tissue samples, demonstrating the specificity of ^{68}Ga-CBP8 for collagen.

Discussion

Fibrosis, regardless of its cause or location, is characterized by excess deposition of collagens, primarily type I collagen, and other extracellular matrix proteins in the parenchyma (20). Indeed, histological proof of fibrosis is predicated on collagen staining. Here, we developed a method for direct molecular PET imaging of type I collagen as a

noninvasive means of detecting and monitoring pulmonary fibrosis. The major advantages of PET are that it enables in vivo visualization of molecular physiological processes in real time, while at the same time allowing quantification by measuring regional concentration of the radiation source. The mass dose of ^{68}Ga-CBP8 required for administration is extremely low (<100 μg per human subject) and like most PET probes is very safe because of the ultralow dose. Targeted PET probes typically have affinities in the low nanomolar range, but such probes typically bind sparse targets like cell surface receptors present at nanomolar concentrations. Our probe ^{68}Ga-CBP8 has low micromolar affinity to type I collagen, but this is sufficient for quantification because collagen is present at concentrations in the 10's of μM during pathological fibrosis.

To generate our probe, we modified a known collagen-specific peptide with a chelator so that it binds the ^{68}Ga ion. Gallium-68 is a positron-emitting radioisotope that is produced from a ^{68}Ge/^{68}Ga generator system, and therefore ^{68}Ga radiopharmacy does not require an onsite cyclotron, similar to ^{99}Mo/^{99m}Tc-based radiopharmacy. The chelation reaction to introduce ^{68}Ga is quantitative driven by the high thermodynamic stability of the resultant ^{68}Ga complex. The 68 min half-life of ^{68}Ga permits facile production of the probe, and the short half-life results in low radiation exposure to the subject. The radiochemistry is amenable to kit formulation and/or automation, with a low barrier to clinical translation. Indeed, there has been a tremendous increase in the number of clinical studies with ^{68}Ga probes over the past year around the world, including within the United States (38).

We demonstrated that PET imaging with our collagen-targeted probe, ^{68}Ga-CBP8, is sensitive enough to detect pulmonary fibrosis in the commonly used BM mouse model. Our study showed that ^{68}Ga-CBP8 provided significantly enhanced PET signal in the lungs of fibrotic mice compared with control mice. Non-specific uptake in the surrounding tissues (such as, muscle, heart, and bone) was similar and low in both fibrotic and control mice. The highest off-target accumulation was in the kidney, but the short half-life of gallium will limit the amount of radiation exposure (39).

When we expanded the ^{68}Ga-CBP8 study to include mice at an early stage of fibrosis, we observed a strong correlation of lung uptake of the probe with hydroxyproline content, indicating the ability of the probe to stage pulmonary fibrosis. The control probe, ^{68}Ga-CBP12, showed similar, low uptake in the lungs of both fibrotic and control mice, demonstrating that the result observed with ^{68}Ga-CBP8 was a result of specific collagen binding.

We further validated the probe in a second model of pulmonary fibrosis with mice in which a host response to injury was exaggerated by increasing the animals' vascular permeability. In this model, a low-dose BM challenge plus a vascular leak-inducing agent produces robust fibrosis, whereas the low-dose BM challenge alone causes only a mild, self-limited injury in control mice (40, 41). This model captures an important aspect of IPF pathogenesis, in which fibrosis is thought to result from an aberrant or exaggerated host responses to relatively common and/or mild environmental injuries, which may be well tolerated and repaired in most people. In this model, PET imaging of collagen with ^{68}Ga-CBP8 successfully identified animals with pulmonary fibrosis, and additionally, detected blunted

disease progression in animals treated with 3G9, a murine antibody targeted to integrin $\alpha_v\beta_6$ that interferes with TGF-β activation, leading to reduced TGF-β signaling.

Our data raise the possibility that ^{68}Ga-CBP8 more readily/avidly binds newly formed collagen in active disease than it does established, mature collagen. For instance, we see relatively low uptake of ^{68}Ga-CBP8 in bone or skin, which are rich in type I collagen. The lungs themselves are rich in collagen and by direct biochemical measurement lung collagen increases 2–3 fold in mouse models of pulmonary fibrosis. We nevertheless see a 6-fold higher probe uptake in fibrotic mouse lungs compared to control lungs, suggestive of higher binding to the collagen newly formed during fibrosis. Similar observations were made in other models of fibrosis with an analogous MRI probe (21–26).

There are two factors that could contribute to the specificity of the probe for newly formed collagen and active fibrosis. The first relates to the structural nature of type I collagen. A single collagen molecule (tropocollagen) is made of three polypeptide strands that assemble into a microfibril triple helix. In normal tissue, these microfibrils interdigitate, are cross-linked and form stable fibrils (42). Therefore, most of the collagen monomers within these fibrils are inaccessible to a molecular probe like ^{68}Ga-CBP8 because most monomers will be inside the fibril and the probe can only access the fibril surface. However, in active fibrosis, collagen production is upregulated and new collagen is not yet fully organized into stable fibrils. As a result, collagen monomers are more accessible to the probe. If confirmed, this property may augment the ability of ^{68}Ga-CBP8 to provide a much-needed assessment of “disease activity” in IPF and other fibrotic diseases.

Whereas HRCT can accurately measure an IPF patient’s disease severity at the time of evaluation, this imaging modality and other currently available measures to monitor IPF patients provide little information about disease activity (that is, how likely that patient’s fibrosis is to worsen in the upcoming weeks and months). If the ability of ^{68}Ga-CBP8 molecular imaging to assess disease activity in pulmonary fibrosis patients is validated, it could improve patient care and clinical research in IPF in several important ways. Progress in IPF patient care and clinical research has been hampered by the substantial heterogeneity of the disease. Although IPF has a very poor prognosis overall, its clinical course in different patients is highly variable (3). Whereas some patients have active disease that quickly progresses to respiratory failure, others have minimally active disease that remains clinically stable for long periods of time (3). The ability to distinguish IPF patients who are worsening rapidly from those who are remaining stable would enable clinicians to individualize patient care plans. Being able to make this distinction would also allow clinical trials of new IPF therapies to enroll subjects more likely to progress during the period of observation, improving the ability of these trials to detect treatment effects. Additionally, since current assessments of IPF usually take 6 or 12 months to show meaningful changes, being able to assess disease activity would enable faster assessments of patient responses to new therapies.

^{68}Ga-CBP8 has moderate affinity for collagen (2.1 μM), which may also result in better sensitivity to fibrosis. For instance, we measured 50 μg hydroxyproline in the left lung of mice. Assuming that all the hydroxyproline arises from collagen and that it comprises ~13% of collagen, this results in a collagen monomer concentration of ~10 μM, which rises in

excess of 25 μM in fibrotic lungs. Thus, in normal lung the collagen concentration is at or below (depending on accessibility to the collagen) the K_d of the probe, which results in poor uptake. However, in fibrosis the target concentration is in excess of the K_d, resulting in increased probe uptake and the observed collagen-concentration dependent uptake of the probe. The results of our study suggest that ^{68}Ga-CBP8 PET may be a useful complement to HRCT for noninvasive characterization of pulmonary fibrosis. HRCT provides a good measure of fibrotic burden, while ^{68}Ga-CBP8 may highlight regions where fibrosis is more active.

An important limitation of the current study is that BM fibrosis in the animal lacks important features of the human disease. The slow and irreversible progression of fibrosis seen in IPF patients is not reproduced in the BM model. Chronic diseases are notoriously difficult to model. IPF is particularly complicated because the etiology and natural history of the disease is unclear, and no single trigger is known that is able to induce “IPF” in animal models.

To assess probe performance in human tissues, we incubated human IPF lung tissue samples with ^{68}Ga-CBP8 and were able to correlate probe uptake with histological findings of IPF in these samples. ^{68}Ga-CBP12 was not sensitive to collagen changes in IPF human tissue samples, which demonstrates the specificity of ^{68}Ga-CBP8 for collagen. Although this pilot study was limited to three patients, the data provide proof-of-principle evidence of the potential of ^{68}Ga-CBP8 PET as an imaging agent for pulmonary fibrosis in humans. The human tissue data support the hypothesis that the probe is more sensitive to newer, less organized collagen. We found that uptake in region of the lung that was characteristic of dense, established subpleural fibrosis with microscopic honeycomb change was higher than in a region reflective of end stage fibroelastosis with cystic honeycomb change. This distinction suggested that as fibrosis becomes end stage, a larger fraction of the matrix is elastin and the collagen is more organized and less available for binding to our probe. The barrier to translate our collagen-binding PET probe into clinic is very low. Unlike other imaging modalities (e.g. MRI, optical), the low mass dose required for PET allows clinical translation under the FDA exploratory investigational new drug (eIND) mechanism on the basis of a single high-dose acute toxicity study in rodents.

Recently, the Food and Drug Administration approved two different therapeutic agents for the treatment of IPF in the United States, pirfenidone and nintedanib, largely based on results from the CAPACITY (43), ASCEND (44) and INPULSIS trials (45). Both drugs slow functional decline and disease progression, and reduce long-term mortality in patients with mild to moderate IPF, highlighting the importance of early diagnosis and initiation of treatment. The usefulness of these drugs in other forms of pulmonary fibrosis is starting to be evaluated, including scleroderma-associated interstitial lung disease, chronic hypersensitivity pneumonitis and radiation pneumonitis. If current anti-fibrotic therapy can slow functional decline and disease progression in fibrotic lung diseases, then early detection of pulmonary fibrosis of any cause and initiation of treatment could benefit patients across this broad category of lung diseases. Because lung architectural distortion may be absent early in the course of fibrotic lung diseases, HRCT often cannot distinguish fibrosis from other pathological processes in the lung. In this regard, our results may represent a consistent

and reliable non-invasive method to detect excess collagen deposition in the lungs, even early in the course of pulmonary fibrosis. This ability of ^{68}Ga-CBP8 molecular imaging, as well as the potential application to assess the rate of progression, or disease activity of pulmonary fibrosis, suggests that translation of this approach to human will benefit patients with IPF and other fibrotic lung diseases.

Materials and Methods

Study design

The objective of this study was to address the clinically unmet need of non-invasive tools to diagnose IPF at early stage, to quantify and stage fibrosis, and to monitor disease progression.

This goal was addressed by (i) evaluating the efficacy and specificity of the probe to detect and stage disease in an established animal model for pulmonary fibrosis (bleomycin), (ii) evaluating the probe efficacy to detect disease and its capacity to monitor treatment response in a second model of pulmonary fibrosis using mice in which a host response to injury has been exaggerated by increased vascular permeability, (iii) and initiating a pilot study to translate these findings using human IPF tissue samples.

All experiments were performed in accordance with the National Institutes of Health guidelines for the Care and Use of Laboratory Animals, with the ARRIVE guidelines, and were approved by the institution's animal care and use committee. Evaluation of ^{68}Ga-CBP8 and ^{68}Ga-CBP12 uptake measurements in animals was performed in a non-blinded fashion. Authors were blinded for histology analysis. Because ^{68}Ga-CBP8 microPET imaging is a new imaging technology, it is difficult to estimate sample size with adequate power. An n = 4 to 13 was selected for these well-controlled models with a low (<10%) error in consecutive studies. Binding studies were conducted using three independent experiments. No samples or animals were excluded from data analyses.

Fresh lung tissue samples were collected from explanted IPF lungs obtained from 3 IPF patients undergoing transplantation. The Partners Human Research Committee Institutional Review Board approved this study. Informed consent was obtained from the patients.

Synthesis of precursors and non-radioactive standards

All chemicals were purchased commercially and used without further purification. The cyclic disulfide peptide precursors of CBP8 and CBP12 (cPep(8) and cPep(12)) were custom-made by American Peptide. The tri-tert-butyl-protected activated ester NODAGA-*N*-hydroxusuccinimide ((ᵗBu)$_3$NODAGA-NHS) was synthesized in-house following a published procedure (47) starting from 1,4,7-triazacyclononane (Chematech).

(ᵗBu)$_3$NODAGA-cPep(x)—Three equivalents of (ᵗBu)$_3$NODAGA-NHS were added to solution of cPep(x) (x=8, 12) in 1 mL dimethylformamide (DMF). The pH of each solution was adjusted to 6.5 using diisopropylethylamine (DIPEA) and the mixtures were stirred at room temperature for 24 hours. (ᵗBu)$_3$NODAGA-cPep(8) and (ᵗBu)$_3$NODAGA-cPep(12) were purified separately by reversed-phase semi-preparative purification (Dynamax HPLC

system, Phenomenex Luna C18 column (5 μm, 250 mm × 21.2 mm), water/acetonitrile gradient (85:15, 60:40 in 30 min) containing 0.1% (v/v) trifluoroacetic acid (TFA); the extinction at 280 nm was monitored for detection). The 2 products had a purity >98% as determined by LC-MS (Agilent 1100 Series apparatus with an LC/MSD trap and Daly conversion dynode detector with UV detection at 220, 254, and 280 nm, Phenomenex Kinetex C18 column (2.6 μm, 100 mm × 4.6 mm), water/acetonitrile gradient (95:5, 5:95 in 10 min) containing 0.1% (v/v) formic acid). $(tBu)_3$NODAGA-cPep(8): Molecular weight for $C_{193}H_{285}N_{37}O_{43}S_2$. MS(ESI) calc: 970.0 [(M+4H)/4]4+; found: 969.9. $(tBu)_3$NODAGA-cPep(12): Molecular weight for $C_{193}H_{285}N_{37}O_{43}S_2$. MS(ESI) calc: 970.0 [(M+4H)/4]4+; found: 969.7.

NODAGA-cPep(x)—In 2 separate reaction vessels, about 20 mg of $(^tBu)_3$NODAGA-cPep(x) (x=8, 12) were dissolved in a 1 mL solution of TFA, methanesulfonic acid, 1-dodecanethiol and H_2O (92:3:3:2). Each reaction mixture was stirred for 2 h. Cold diethyl ether was added to precipitate out the solids. The mixtures were centrifuged, and the supernatant removed. The solids were washed with diethyl ether and dried to give the product as white solids. NODAGA-cPep(8) and NODAGA-cPep(12) were purified by reversed-phase semi-preparative purification. The 2 products had a purity >98% as determined by LC-MS. NODAGA-cPep(8): Molecular weight for $C_{157}H_{213}N_{37}O_{43}S_2$, MS(ESI) calc: 843.8 $[(M+4H)/4]^{4+}$; found: 843.4. NODAGA-cPep(12): Molecular weight for $C_{157}H_{213}N_{37}O_{43}S_2$, MS(ESI) calc: 843.8 $[(M+4H)/4]^{4+}$; found: 843.5.

$^{69/71}$Ga-NODAGA-cPep(8)—3 mg of NODAGA-cPep(8) were dissolved in 2 mL of sodium acetate buffer (20 mM, pH=4.1). A sample of 296 μL of a 3 mM $^{69/71}Ga(NO_3)_3$ was added in the vessel and the reaction mixture was stirred at 60 °C for 20 min. $^{69/71}$Ga-NODAGA-cPep(8) was purified by reversed-phase semi-preparative purification. The product had a purity >98% as determined by LC-MS. Molecular weight for $C_{157}H_{210}GaN_{37}O_{43}S_2$, MS(ESI) calc: 860.3 $[(M+4H)/4]^{4+}$; found: 860.5.

$^{69/71}$Ga-NODAGA-cPep(12)—5 mg of NODAGA-cPep(12) were dissolved in 2 mL of sodium acetate buffer (20 mM, pH=4.1). A sample of 1.5 mL of a 3 mM $^{69/71}Ga(NO_3)_3$ was added in the vessel and the reaction mixture was stirred at 60 °C for 20 min. $^{69/71}$Ga-NODAGA-cPep(12) was purified by reversed-phase semi-preparative purification. The product had a purity >98% as determined by LC-MS. Molecular weight for $C_{157}H_{210}GaN_{37}O_{43}S_2$, MS(ESI) calc: 860.3 $[(M+4H)/4]^{4+}$; found: 860.5.

Radiosynthesis

$^{68}GaCl_3$ was obtained from a SnO_2-based $^{68}Ge/^{68}Ga$ generators (iThemba Labs). $^{68}GaCl_3$ (10 mCi, in 0.5 mL HCl (0.6 M)) was diluted with 200 μL of pH 5 sodium acetate (3 M) to reach pH 4.1. A sample of 180 μL of the $^{68}GaCl_3$ solution was combined to 5 μL of a 0.1 mM (NODAGA)-cPep(8) or (NODAGA)-cPep(12) solution (in sodium acetate pH 4.1) and the reaction mixture was heated at 60 °C for 5 min and purified by Sep-Pak C18 cartridge (Waters) to remove any radiometal impurities (germanium-68 breakthrough). The radiochemical purity of the final solution of CBP8 and CBP12 was ≥99% as determined by radio-HPLC analysis (Agilent 1100 Series HPLC unit with a Carroll/Ramsey radiation

detector with a silicon PIN photodiode and with UV detection at 254 nm, Phenomenex Luna C18 column (2.6 μm, 100 mm × 4.6 mm), water/acetonitrile gradient (95:5, 5:95 in 10 min) containing 0.1% (v/v) TFA). Specific activities ranged from 324 to 462 GBq/μmol.

Collagen binding

Binding isotherms were obtained using the cold version of the probes ($^{69/71}$Ga-CBP8 or $^{69/71}$Ga-CBP12) by following a method previously reported (21).

Animal model and probe administration

In the standard-dose BM model (48), pulmonary fibrosis was induced in 10-week-old male C57/BL6 mice, (20–28 g, Charles River Laboratories) by transtracheal administration of BM (2.5 U/kg) in 50 μL of PBS under direct vision using a small cervical incision. In the low dose bleomycin model associated with a vascular leak agent (FTY720) (40), adult male C57Bl/6 mice, 7–8 weeks old (~ 25 g, Charles River Laboratories) were administered a single intratracheal dose of bleomycin at 0.1 U/kg (low dose), in a total volume of 50 μL sterile saline. FTY720 was administered intraperitoneally to the mice at 1mg/kg three times a week. To effect treatment in the low dose bleomycin, vascular leak model, the therapeutic murine antibody 3G9 (anti-$\alpha_v\beta_6$-blocking antibody) and 1E6 (matched isotype control antibody) were used (49). All administrations of FTY720 and antibodies were initiated on day 0, ~30 min before bleomycin challenge and continued throughout the duration of the experiments.

Small animal PET-CT imaging and analysis

Animals were placed in a small-animal PET/SPECT/CT scanner (Triumph; TriFoil Imaging), equipped with inhalation anesthesia and heating pad. Each animal was anesthetized with isoflurane (4% for induction, 1–1.5% for maintenance in medical air). After placement of an in-dwelling catheter in the femoral vein for probe administration, mice were positioned in the PET-CT and probe was given as a bolus. Dynamic imaging was performed for 120 minutes for sham and BM-mice (day 14) injected with ^{68}Ga-CBP8 and ^{68}Ga-CBP12. Static imaging was performed on mice treated with BM (day 7), FTY alone, LDB, LDBVL, LDBVL+3G9 and LDBVL+1E6, acquisitions were collected 50 minutes after ^{68}Ga-CBP8 injection and for 30 minutes. A whole body CT was obtained either immediately before or immediately after the PET acquisition, and the mice were then euthanized at 150 minutes post injection and the organs taken for biodistribution analysis. Instrument calibration was performed with phantoms containing small known amounts of radioactivity. Isotropic (0.3 mm) CT images were acquired over 6 min with 512 projections with 3 frames per projection (exposure time per frame,~200 msec; peak tube voltage, 70 kV; tube current, 177 mA). PET and CT images were reconstructed using the LabPET software (TriFoil Imaging) and the CT data were used to provide attenuation correction for the PET reconstructions. The PET data were reconstructed using a maximum-likelihood expectation-maximization (MLEM) algorithm run over 30 iterations to a voxel size of 0.5 × 0.5 × 0.6 mm^3. For the pharmacokinetic analyses, the PET data were reconstructed in 1 min (first 10 frames), 3 min (next 10 frames), and 10 min (last 8–10 frames) intervals out to 120 min post injection. Reconstructed PET/CT data were quantitatively evaluated using AMIDE software package (50). For each PET scan, volumes of interest (VOIs) were drawn over major organs

on decay-corrected whole body coronal images. The radioactivity concentration within organs was obtained from mean pixel values within the VOI volume and converted to counts per milliliter per minute and then divided by the injected dose (ID) to obtain an imaging VOI-derived percentage of the injected radioactive dose per cubic centimeter of tissue (%ID/cc). Size of the VOI was about 65 mm^3 for the lungs, 53 mm^3 for the heart and 20 mm^3 for the muscle.

Biodistribution protocol

From all animals were collected the left lung, blood, urine, heart, liver, left rectus femoris muscle, spleen, small intestine, kidneys, left femur bone. The tissues were weighed, and radioactivity in each tissue was measured on a gamma counter (Wizard2 Auto Gamma, PerkinElmer). Tracer distribution was presented as %ID/g for all organs. The radioactivity in the lung was reported as percent injected dose per lung.

Human lung tissues were collected within 1 hour of resection. Samples were weighted (70 to 100 mg per sample), cut in small pieces and introduced in an eppendorf tube containing a solution of ^{68}Ga-CBP8 (50 to 75 kBq) in PBS (1 mL). The mixture was shaken for 2 hours at room temperature. After centrifugation, supernatant (sup-1) was removed, kept for further analysis and tissue samples were washed with 1 mL of PBS, this procedure was repeated twice for each sample. Wash solutions (wash-1 and wash-2) were kept for further analysis. Activities in tissue samples and in solutions sol-1, wash-1 and wash-2 were measured on a gamma counter. Activity in the tissue was presented as %Lung uptake, defined by activity in the tissue measured by gamma counter divided by total of activity (from tissue, sup-1, wash-1 and wash-2).

Ex vivo analysis

Mouse lung tissues (right lungs) were inflated and fixed with 10% formalin, embedded in paraffin, cut into 5 μm sections. Tissue sections were stained with Hematoxylin, Eosin and Picrosirius Red with a counterstain of Fast Green (Fig. 4A). Images were acquired using a Nikon TE-2000 microscope (×10 and ×40 magnification). Sirius Red stained sections were analyzed by a pathologist, who was blinded to the study, to score the amount of lung disease according to the method of Ashcroft (28). In addition, % Sirius Red was quantified from the histology images using ImageJ as per our standard procedures (26). Human lung tissues were obtained just adjacent to fresh tissues for probe incubation and were fixed in 10% formalin, embedded in paraffin and cut into 5 μm sections. Tissue sections were stained with Hematoxylin, Eosin, Picrosirius Red, Masson Trichrome and Verhoeff's elastic stain. Slides were scanned using a digital slide scanner (Aperio CS2, Leica Biosystem).

Quantification of collagen

Hydroxyproline in tissue was quantified by HPLC analysis of tissue acid digests as previously described. Hydroxyproline is expressed as amount per lung (51).

Statistics

Unless otherwise noted, the results are expressed as means ± SEM (with n = 4–13 mice per group). Statistical analyses were performed with GraphPad Prism 7 software (LA Jolla, CA).

A one-way ANOVA, followed by post hoc Tukey tests with two-tailed distribution was used for analyzing the data between different groups. A p value of less than 0.05 was considered significant.

Supplementary Material

Refer to Web version on PubMed Central for supplementary material.

Acknowledgments

We thank Dr. O. M. Evbuomwan and Dr J. Hooker for use of $^{68}Ge/^{68}Ga$ generator; Dr H. Chen, Dr P. Waghorn and Dr D. Dos Santos Ferreira and Dr H. Diyabalanage for assistance during animal set up; S.E. Conley for scanning slides of human lung tissues; M.K. Selig for performing the Electron Microscopy imaging; the Wellman Center for Photomedicine Photopathology core for the work on the human lung tissues.

Funding: Supported by the National Heart and Lung and Blood Institute (NHLBI) R01HL116315. PD was supported by the Harvard/MGH Nuclear Medicine Training program, which is funding by the US Dept. of Energy (DE-SC0008430). Instrumentation support from the National Center for Research Resources (micro-PET/SPECT/CT system, RR029495) and the Office of Director (ICP-QQQ, OD010650) is acknowledged.

References and Notes

1. Bjoraker JA, Ryu JH, Edwin MK, Myers JL, Tazelaar HD, Schroeder DR, Offord KP. Prognostic significance of histopathologic subsets in idiopathic pulmonary fibrosis. Am J Respir Crit Care Med. 1998; 157:199. [PubMed: 9445300]
2. King TE, Schwarz MI, Brown K, Tooze JA, Colby TV, Waldron JA Jr, Flint A, Thurlbeck W, Cherniack RM. Idiopathic pulmonary fibrosis: relationship between histopathologic features and mortality. Am J Respir Crit Care Med. 2001; 164:1025. [PubMed: 11587991]
3. Raghu G, Collard HR, Egan JJ, Martinez FJ, Behr J, Brown KK, Colby TV, Cordier JF, Flaherty KR, Lasky JA, Lynch DA, Ryu JH, Swigris JJ, Wells AU, Ancochea J, Bouros D, Carvalho C, Costabel U, Ebina M, Hansell DM, Johkoh T, Kim DS, King TE Jr, Kondoh Y, Myers J, Muller NL, Nicholson AG, Richeldi L, Selman M, Dudden RF, Griss BS, Protzko SL, Schunemann HJ. An official ATS/ERS/JRS/ALAT statement: idiopathic pulmonary fibrosis: evidence-based guidelines for diagnosis and management. Am J Respir Crit Care Med. 2011; 183:788. [PubMed: 21471066]
4. Hunninghake GW, Zimmerman MB, Schwartz DA, King TE Jr, Lynch J, Hegele R, Waldron J, Colby T, Muller N, Lynch D, Galvin J, Gross B, Hogg J, Toews G, Helmers R, Cooper JA Jr, Baughman R, Strange C, Millard M. Utility of a lung biopsy for the diagnosis of idiopathic pulmonary fibrosis. Am J Respir Crit Care Med. 2001; 164:193. [PubMed: 11463586]
5. Souza CA, Muller NL, Flint J, Wright JL, Churg A. Idiopathic pulmonary fibrosis: spectrum of high-resolution CT findings. AJR Am J Roentgenol. 2005; 185:1531. [PubMed: 16304008]
6. Hutchinson JP, Fogarty AW, McKeever TM, Hubbard RB. In-Hospital Mortality after Surgical Lung Biopsy for Interstitial Lung Disease in the United States. 2000 to 2011. Am J Respir Crit Care Med. 2016; 193:1161. [PubMed: 26646481]
7. Jenkins RG, Simpson JK, Saini G, Bentley JH, Russell AM, Braybrooke R, Molyneaux PL, McKeever TM, Wells AU, Flynn A. Longitudinal change in collagen degradation biomarkers in idiopathic pulmonary fibrosis: an analysis from the prospective, multicentre PROFILE study. Lancet Respir Med. 2015; 3:462. [PubMed: 25770676]
8. Gibbons MA, MacKinnon AC, Ramachandran P, Dhaliwal K, Duffin R, Phythian-Adams AT, van Rooijen N, Haslett C, Howie SE, Simpson AJ. Ly6Chi monocytes direct alternatively activated profibrotic macrophage regulation of lung fibrosis. Am J Respir Crit Care Med. 2012; 184:569.
9. Withana NP, Ma X, McGuire HM, Verdoes M, van der Linden WA, Ofori LO, Zhang R, Li H, Sanman LE, Wei K. Non-invasive Imaging of Idiopathic Pulmonary Fibrosis Using Cathepsin Protease Probes. Scientific reports. 2016; 6:19755. [PubMed: 26797565]
10. Ambrosini V, Zompatori M, De Luca F, Antonia D, Allegri V, Nanni C, Malvi D, Tonveronachi E, Fasano L, Fabbri M, Fanti S. 68Ga-DOTANOC PET/CT allows somatostatin receptor imaging in

idiopathic pulmonary fibrosis: preliminary results. J Nucl Med. 2010; 51:1950. [PubMed: 21078794]

11. Lebtahi R, Moreau S, Marchand-Adam S, Debray MP, Brauner M, Soler P, Marchal J, Raguin O, Gruaz-Guyon A, Reubi JC, Le Guludec D, Crestani B. Increased uptake of 111In-octreotide in idiopathic pulmonary fibrosis. J Nucl Med. 2006; 47:1281. [PubMed: 16883006]
12. Munger JS, Huang X, Kawakatsu H, Griffiths MJD, Dalton SL, Wu J, Pittet JF, Kaminski N, Garat C, Matthay MA, Rifkin DB, Sheppard D. A mechanism for regulating pulmonary inflammation and fibrosis: the integrin alpha(v)beta6 binds and activates latent TGFbeta. Cell. 1999; 96:319. [PubMed: 10025398]
13. Wong W. Limiting TGF-β signaling to prevent fibrosis. Sci Signal. 2015; 8:ec34.
14. Froese AR, Shimbori C, Bellaye PS, Ask K, Inman M, Obex S, Fatima S, Jenkins G, Gauldie J, Kolb M. Stretch Induced Activation of TGF-β1 in Pulmonary Fibrosis. Am J Respir Crit Care Med. 2016; 194:84. [PubMed: 26771871]
15. John AE, Luckett JC, Tatler AL, Awais RO, Desai A, Habgood A, Ludbrook S, Blanchard AD, Perkins AC, Jenkins RG. Preclinical SPECT/CT imaging of αvβ6 integrins for molecular stratification of idiopathic pulmonary fibrosis. J Nucl Med. 2013; 54:2146. [PubMed: 24167080]
16. Reed NI, Jo H, Chen C, Tsujino K, Arnold TD, DeGrado WF, Sheppard D. The αvβ1 integrin plays a critical in vivo role in tissue fibrosis. Science translational medicine. 2015; 7:288ra79.
17. Win T, Lambrou T, Hutton BF, Kayani I, Screaton NJ, Porter JC, Maher TM, Endozo R, Shortman RI, Lukey P, Groves AM. 18F-Fluorodeoxyglucose positron emission tomography pulmonary imaging in idiopathic pulmonary fibrosis is reproducible: implications for future clinical trials. Eur J Nucl Med Mol Imaging. 2012; 39:521. [PubMed: 22258710]
18. Win T, Thomas BA, Lambrou T, Hutton BF, Screaton NJ, Porter JC, Maher TM, Endozo R, Shortman RI, Afaq A. Areas of normal pulmonary parenchyma on HRCT exhibit increased FDG PET signal in IPF patients. Eur J Nucl Med Mol Imaging. 2014; 41:337. [PubMed: 23942907]
19. Umeda Y, Demura Y, Morikawa M, Anzai M, Kadowaki M, Ameshima S, Tsuchida T, Tsujikawa T, Kiyono Y, Okazawa H. Prognostic Value of Dual-Time-Point 18F-FDG PET for Idiopathic Pulmonary Fibrosis. J Nucl Med. 2015; 56:1869. [PubMed: 26359263]
20. Wynn TA, Ramalingam TR. Mechanisms of fibrosis: therapeutic translation for fibrotic disease. Nat Med. 2012; 18:1028. [PubMed: 22772564]
21. Caravan P, Das B, Dumas S, Epstein FH, Helm PA, Jacques V, Koerner S, Kolodziej A, Shen L, Sun WC, Zhang Z. Collagen-targeted MRI contrast agent for molecular imaging of fibrosis. Angew Chem Int Ed Engl. 2007; 46:8171. [PubMed: 17893943]
22. Helm PA, Caravan P, French BA, Jacques V, Shen L, Xu Y, Beyers RJ, Roy RJ, Kramer CM, Epstein FH. Postinfarction myocardial scarring in mice: molecular MR imaging with use of a collagen-targeting contrast agent. Radiology. 2008; 247:788. [PubMed: 18403626]
23. Farrar CT, DePeralta DK, Day H, Rietz TA, Wei L, Lauwers GY, Keil B, Subramaniam A, Sinskey AJ, Tanabe KK, Fuchs BC, Caravan P. 3D molecular MR imaging of liver fibrosis and response to rapamycin therapy in a bile duct ligation rat model. J Hepatol. 2015; 63:689. [PubMed: 26022693]
24. Polasek M, Fuchs BC, Uppal R, Schühle DT, Alford JK, Loving GS, Yamada S, Wei L, Lauwers GY, Guimaraes AR, Tanabe KK, Caravan P. Molecular MR imaging of liver fibrosis: A feasibility study using rat and mouse models. J Hepatol. 2012; 57:549. [PubMed: 22634342]
25. Fuchs BC, Wang H, Yang Y, Wei L, Polasek M, Schühle DT, Lauwers GY, Parkar A, Sinskey AJ, Tanabe KK. Molecular MRI of collagen to diagnose and stage liver fibrosis. J Hepatol. 2013; 59:992. [PubMed: 23838178]
26. Caravan P, Yang Y, Zachariah R, Schmitt A, Mino-Kenudson M, Chen HH, Sosnovik DE, Dai G, Fuchs BC, Lanuti M. Molecular magnetic resonance imaging of pulmonary fibrosis in mice. Am J Respir Cell Mol Biol. 2013; 49:1120. [PubMed: 23927643]
27. Blodgett TM, Meltzer CC, Townsend DW. PET/CT: form and function. Radiology. 2007; 242:360. [PubMed: 17255408]
28. Ashcroft T, Simpson JM, Timbrell V. Simple method of estimating severity of pulmonary fibrosis on a numerical scale. J Clin Pathol. 1988; 41:467. [PubMed: 3366935]

29. Srivastava AK, Khare P, Nagar HK, Raghuwanshi N, Srivastava R. Hydroxyproline: A Potential Biochemical Marker and Its Role in the Pathogenesis of Different Diseases. Curr Protein Pept Sci. 2016; 17:596. [PubMed: 26916157]
30. Selman M, King TE, Pardo A. Idiopathic pulmonary fibrosis: prevailing and evolving hypotheses about its pathogenesis and implications for therapy. Ann Intern Med. 2001; 134:136. [PubMed: 11177318]
31. McKeown S, Richter AG, O'Kane C, McAuley DF, Thickett D. MMP expression and abnormal lung permeability are important determinants of outcome in IPF. Eur Respir J. 2009; 33:77. [PubMed: 18829682]
32. Lawson WE, Cheng DS, Degryse AL, Tanjore H, Polosukhin VV, Xu XC, Newcomb DC, Jones BR, Roldan J, Lane KB. Endoplasmic reticulum stress enhances fibrotic remodeling in the lungs. Proc Natl Acad Sci USA. 2011; 108:10562. [PubMed: 21670280]
33. Shea BS, Brooks SF, Fontaine BA, Chun J, Luster AD, Tager AM. Prolonged exposure to sphingosine 1–phosphate receptor-1 agonists exacerbates vascular leak, fibrosis, and mortality after lung injury. Am J Respir Cell Mol Bio. 2010; 43:662. [PubMed: 20081052]
34. Burns HD, Van Laere K, Sanabria-Bohórquez S, Hamill TG, Bormans G, Eng W-s, Gibson R, Ryan C, Connolly B, Patel S. [18F] MK-9470, a positron emission tomography (PET) tracer for in vivo human PET brain imaging of the cannabinoid-1 receptor. Proc Natl Acad Sci. 2007; 104:9800. [PubMed: 17535893]
35. Lambrou T, Groves AM, Erlandsson K, Screaton N, Endozo R, Win T, Porter JC, Hutton BF. The importance of correction for tissue fraction effects in lung PET: preliminary findings. Eur J Nucl Med Mol Imaging. 2011; 38:2238. [PubMed: 21874321]
36. Horan GS, Wood S, Ona V, Li DJ, Lukashev ME, Weinreb PH, Simon KJ, Hahm K, Allaire NE, Rinaldi NJ. Partial inhibition of integrin αvβ6 prevents pulmonary fibrosis without exacerbating inflammation. Am J Respir Crit Care Med. 2008; 177:56. [PubMed: 17916809]
37. Puthawala K, Hadjiangelis N, Jacoby SC, Bayongan E, Zhao Z, Yang Z, Devitt ML, Horan GS, Weinreb PH, Lukashev ME, Violette SM, Grant KS, Colarossi C, Formenti SC, Munger JS. Inhibition of integrin alpha(v)beta6, an activator of latent transforming growth factor-beta, prevents radiation-induced lung fibrosis. Am J Respir Crit Care Med. 2008; 177:82. [PubMed: 17916808]
38. Banerjee SR, Pomper MG. Clinical Applications of Gallium-68. Appl Radiat Isot. 2013; 0:2.
39. Afshar-Oromieh A, Hetzheim H, Kratochwil C, Benesova M, Eder M, Neels OC, Eisenhut M, Kübler W, Holland-Letz T, Giesel FL. The Theranostic PSMA Ligand PSMA-617 in the Diagnosis of Prostate Cancer by PET/CT: Biodistribution in Humans, Radiation Dosimetry, and First Evaluation of Tumor Lesions. J Nucl Med. 2015; 56:1697. [PubMed: 26294298]
40. Shea BS, Brooks SF, Fontaine BA, Chun J, Luster AD, Tager AM. Prolonged exposure to sphingosine 1–phosphate receptor-1 agonists exacerbates vascular leak, fibrosis, and mortality after lung injury. Am J Respir Cell Mol Bio. 2010; 43:662. [PubMed: 20081052]
41. Shea BS, Tager AM. Role of the lysophospholipid mediators lysophosphatidic acid and sphingosine 1-phosphate in lung fibrosis. Proc Am Thorac Soc. 2012; 9:102. [PubMed: 22802282]
42. Starborg T, Lu Y, Kadler KE, Holmes DF. Electron microscopy of collagen fibril structure in vitro and in vivo including three-dimensional reconstruction. Methods Cell Biol. 2008; 88:319. [PubMed: 18617041]
43. Noble PW, Albera C, Bradford WZ, Costabel U, Glassberg MK, Kardatzke D, King TE, Lancaster L, Sahn SA, Szwarcberg J, Valeyre D, du Bois RM. Pirfenidone in patients with idiopathic pulmonary fibrosis (CAPACITY): two randomised trials. Lancet. 2011; 377:1760. [PubMed: 21571362]
44. King TE Jr, Bradford WZ, Castro-Bernardini S, Fagan EA, Glaspole I, Glassberg MK, Gorina E, Hopkins PM, Kardatzke D, Lancaster L, Lederer DJ, Nathan SD, Pereira CA, Sahn SA, Sussman R, Swigris JJ, Noble PW. A phase 3 trial of pirfenidone in patients with idiopathic pulmonary fibrosis. N Engl J Med. 2014; 370:2083. [PubMed: 24836312]
45. Richeldi L, du Bois RM, Raghu G, Azuma A, Brown KK, Costabel U, Cottin V, Flaherty KR, Hansell DM, Inoue Y. Efficacy and safety of nintedanib in idiopathic pulmonary fibrosis. N Engl J Med. 2014; 370:2071. [PubMed: 24836310]

46. McGrath JC, Drummond GB, McLachlan EM, Kilkenny C, Wainwright CL. Guidelines for reporting experiments involving animals: the ARRIVE guidelines. Br J Pharmacol. 2010; 160:1573. [PubMed: 20649560]

47. Levy SG, Jacques V, Zhou KL, Kalogeropoulos S, Schumacher K, Amedio JC, Scherer JE, Witowski SR, Lombardy R, Koppetsch K. Development of a multigram asymmetric synthesis of 2-(R)-2-(4,7,10-tris tert-Butylcarboxymethyl-1,4,7,10-tetraazacyclododec-1-yl)-pentanedioic acid, 1-tert-butyl ester, (R)-tert-bu4-DOTAGA. Org Process Res Dev. 2009; 13:535.

48. Moeller A, Ask K, Warburton D, Gauldie J, Kolb M. The bleomycin animal model: a useful tool to investigate treatment options for idiopathic pulmonary fibrosis? Int J Biochem Cell Biol. 2008; 40:362. [PubMed: 17936056]

49. Li S, McGuire MJ, Lin M, Liu YH, Oyama T, Sun X, Brown KC. Synthesis and characterization of a high-affinity {alpha}v{beta}6-specific ligand for in vitro and in vivo applications. Mol Cancer Ther. 2009; 8:1239. [PubMed: 19435868]

50. Loening AM, Gambhir SS. AMIDE: a free software tool for multimodality medical image analysis. Mol Imaging. 2003; 2:131. [PubMed: 14649056]

51. Hutson PR, Crawford ME, Sorkness RL. Liquid chromatographic determination of hydroxyproline in tissue samples. J Chromatogr B, Analyt Technol Biomed Life Sci. 2003; 791:427.

One Sentence Summary

Positron emission tomography with a probe targeting type I collagen enables detection, staging, and treatment response monitoring in lung fibrosis.

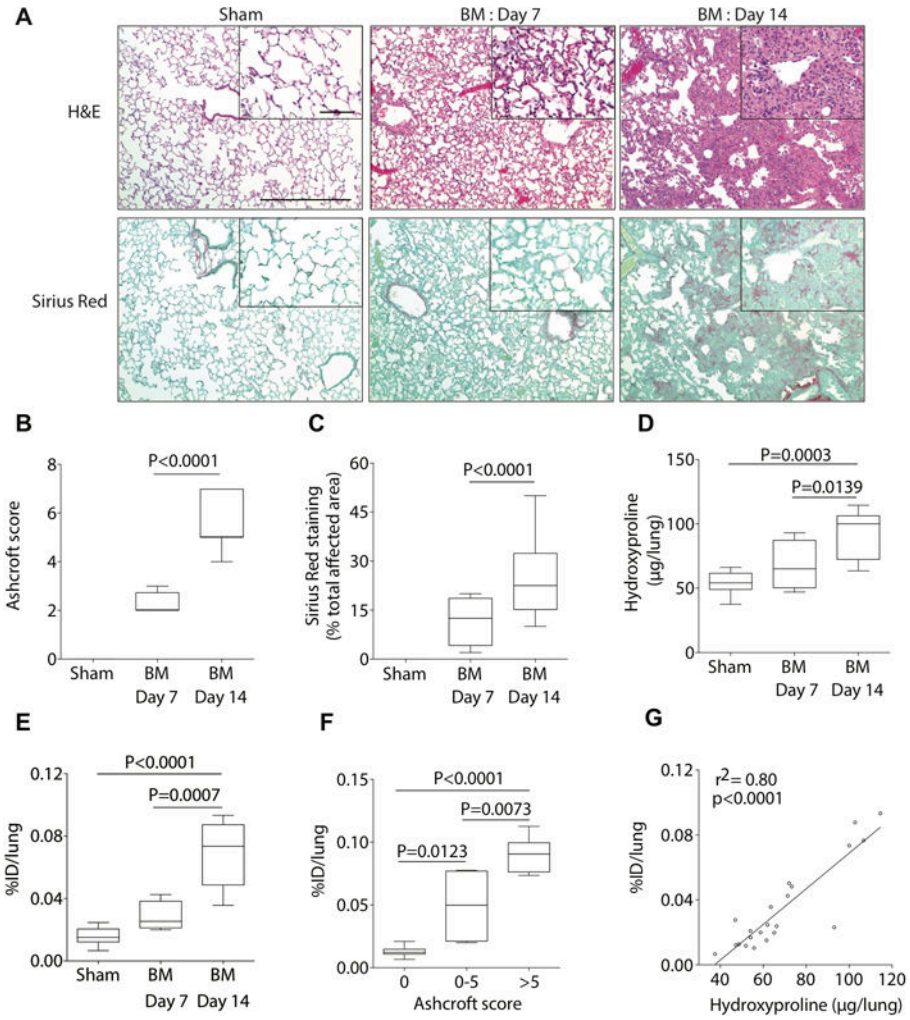

Fig. 1. Probe ^{68}Ga-CBP8 monitors disease progression in the bleomycin mouse model of pulmonary fibrosis

(A) Representative images of lung tissue stained with hematoxylin and eosin (H&E) and Sirius red (×10, scale bar, 300 µm) for sham and BM-treated mice at day 7 and day 14 after BM instillation; higher-magnification views are also displayed (×40, scale bar, 60 µm). (A to D) Disease progresses in a stepwise fashion as determined by histological Ashcroft scoring of lung fibrosis (B), by histological quantification of the area affected by disease (C) and by hydroxyproline (Hyp) analysis (D). (E) Ex-vivo lung uptake of ^{68}Ga-CBP8 increases with disease progression in the BM-treated mice; 5-fold higher in BM-mice 14 days after instillation than in sham animals, 1.5 higher uptake in BM-mice 14 days after instillation compared with BM-mice 7 days after instillation. (F) Correlation of ex-vivo ^{68}Ga-CBP8 lung uptake and Ashcroft score. (G) Correlation between ex-vivo lung uptake of ^{68}Ga-CBP8 and lung hydroxyproline. Data were analyzed with one-way ANOVA, followed by post hoc Tukey tests with two-tailed distribution. For panels B-F, data are displayed as box plots with the dark band inside the box representing the mean, the bottom and top of the box the first and third quartiles, and the whiskers the minimum and maximum values. For all of the experiments shown in this figure: n=11 for sham, n=4 for BM-treated mice at day 7, and n=7 for BM-treated mice at day 14.

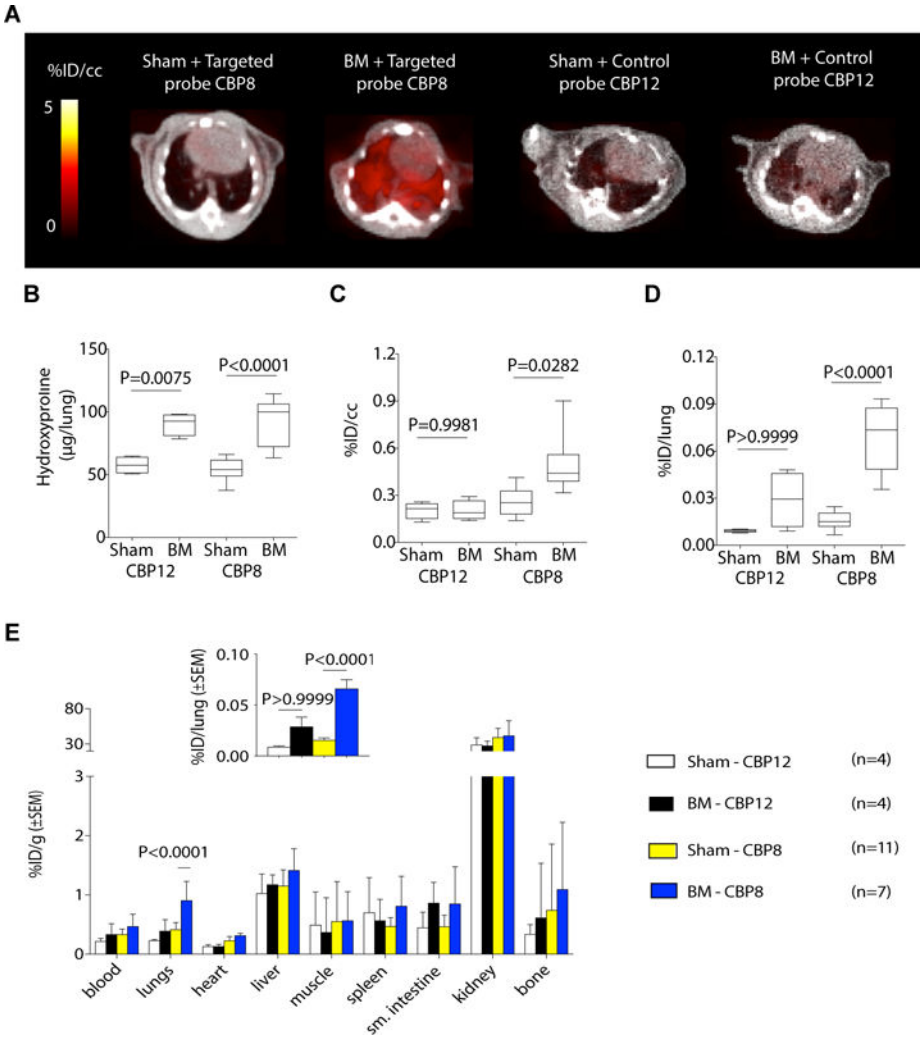

Fig. 2. ^{68}Ga-CBP8 is specifically taken up by fibrotic but not healthy lungs (bleomycin model)

(A) Representative fused PET-CT images show specific accumulation of ^{68}Ga-CBP8 (left images) in fibrotic but not control lungs; ^{68}Ga-CBP12 (right images) showed no preferential uptake in the lungs of BM-treated mice compared to control mice. Greyscale image shows CT image, color scale image shows PET image from integrated data 50–80 min after probe injection. B. Hydroxyproline level was significantly higher in fibrotic BM-treated animals than in the sham-treated animals. C. PET activity values for ^{68}Ga-CBP8 and ^{68}Ga-CBP12 in sham and BM-treated mice (50–80 min after injection). Data are expressed as percent injected dose per cubic centimeter of tissue (%ID/cc). Data show significantly higher uptake in fibrotic lungs with ^{68}Ga-CBP8. D. Ex vivo uptake of ^{68}Ga-CBP8 and ^{68}Ga-CBP12 in lungs from sham and BM-treated mice 150 min after injection expressed as %ID per lung. E. Distribution of ^{68}Ga-CBP8 and ^{68}Ga-CBP12, expressed as percent injected dose per gram of tissue (%ID/g), (mean ± standard error) in various organs was similar except in fibrotic lungs. (Inset) The same data as in E expressed as %ID/lung. Data were analyzed using one-way ANOVA, followed by post hoc Tukey tests with two-tailed distribution. For all of the experiments shown in this figure: n=4 for sham injected with ^{68}Ga-CBP12, n=4 for BM-treated mice injected with ^{68}Ga-CBP12, n=11 for sham injected with ^{68}Ga-CBP8 and n=7

for BM-treated mice injected with ^{68}Ga-CBP8. For panels B–D, data are displayed as box plots with the dark band inside the box representing the mean, the bottom and top of the box the first and third quartiles, and the whiskers the minimum and maximum values.

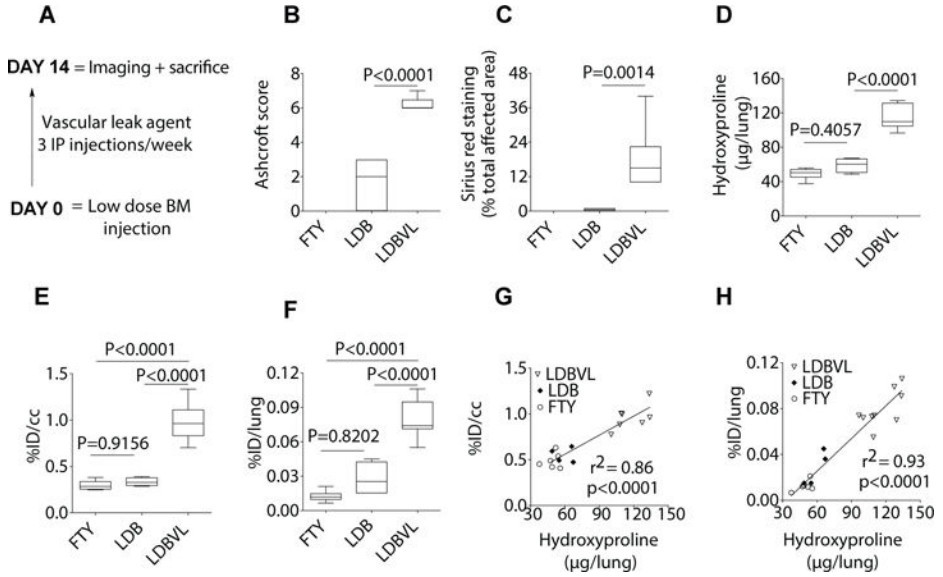

Fig. 3. ^{68}Ga-CBP8 detects and stages disease in a mouse model of pulmonary fibrosis with enhanced vascular permeability

(A) Treatment scheme for the LDBVL group, which was treated with a low dose of BM (0.1 U/kg) and the vascular leak agent FTY720. (B to F) Mice were treated with a very low dose of BM (LDB), the vascular leak agent FTY720 (FTY), or both, administered together (LDBVL). The LDBVL, but not LDB or FTY, group exhibited a fibrotic response as determined by histological Ashcroft scoring of lung fibrosis (B), by Sirius red staining (% total area affected by disease) (C) and by hydroxyproline (Hyp) analysis (D). Data show significantly higher uptake of ^{68}Ga-CBP8 in lungs of LDBVL animals compared to FTY or LDB animals as quantified by PET data (E) and by ex vivo uptake (F). (G and H) Correlations between hydroxyproline levels and %ID/cc (G) and %ID/lung (H). Data were analyzed using one-way ANOVA, followed by post hoc Tukey tests with two-tailed distribution. For all of the experiments shown in this figure: n=6 for the FTY group, n=4 for the LDB group, n=9 for the LDBVL. For panels B–F, data are displayed as box plots with the dark band inside the box representing the mean, the bottom and top of the box the first and third quartiles, and the whiskers the minimum and maximum values.

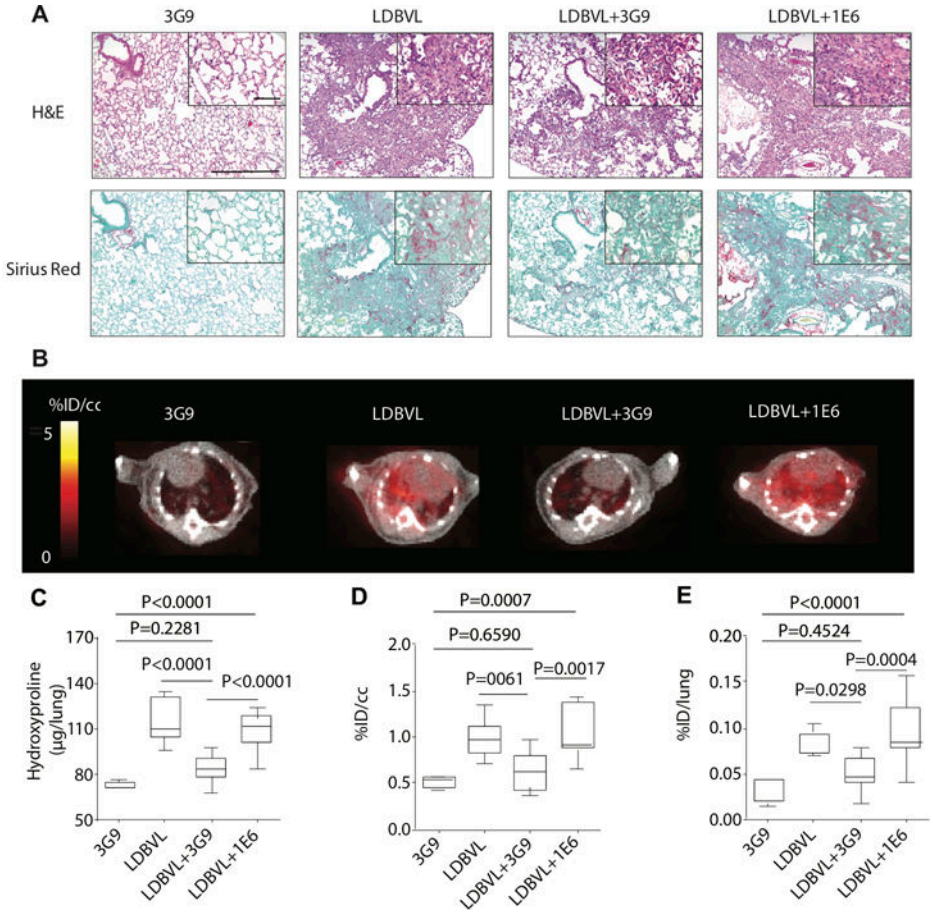

Fig. 4. ^{68}Ga-CBP8 PET allows monitoring of the response to anti-fibrotic therapy in mice

(A) Representative images of lung tissue stained with hematoxylin and eosin (H&E) and Sirius red (×10, scale bar, 300 µm) for mice treated with 3G9 only (n=5), for mice treated with a low dose of BM and FTY720 (LDBVL, n=9), for LDBVL mice receiving 3G9, LDBVL+3G9 (n=11) and for LDBVL mice receiving 1E6, LDBVL+1E6 (n=11); higher-magnification views are also displayed (×40, scale bar, 60 µm). (B) Representative fused PET-CT images show specific accumulation of ^{68}Ga-CBP8 in the lungs of mice from the LDBVL and LDBVL+1E6 groups and but low PET signal in the lungs of the control 3G9 or treated LDBVL+3G9 groups. Greyscale image shows CT image, color scale image shows PET image from integrated data 50–80 min after probe injection. (C) Hydroxyproline content was significantly higher in animals from the LDBVL and LDBVL+1E6 groups than in animals from the 3G9 and LDBVL+3G9 groups showing that the treatment of LDBVL animals with 3G9 is preventive against fibrosis. The treatment of LDBVL animals with 1E6 has no effect on fibrosis. (D) and (E) Similar effects were seen for quantitative PET data (D) and ex vivo uptake in the lungs. Data were analyzed using one-way ANOVA, followed by post hoc Tukey tests with two-tailed distribution. For panels C–E, data are displayed as box plots with the dark band inside the box representing the mean, the bottom and top of the box the first and third quartiles, and the whiskers the minimum and maximum values. For all of the experiments shown in this figure: n=5 for the 3G9 group, n=9 for the LDBVL group, n=11 for the LDBVL+3G9 and n=11 for the LDBVL+1E6.

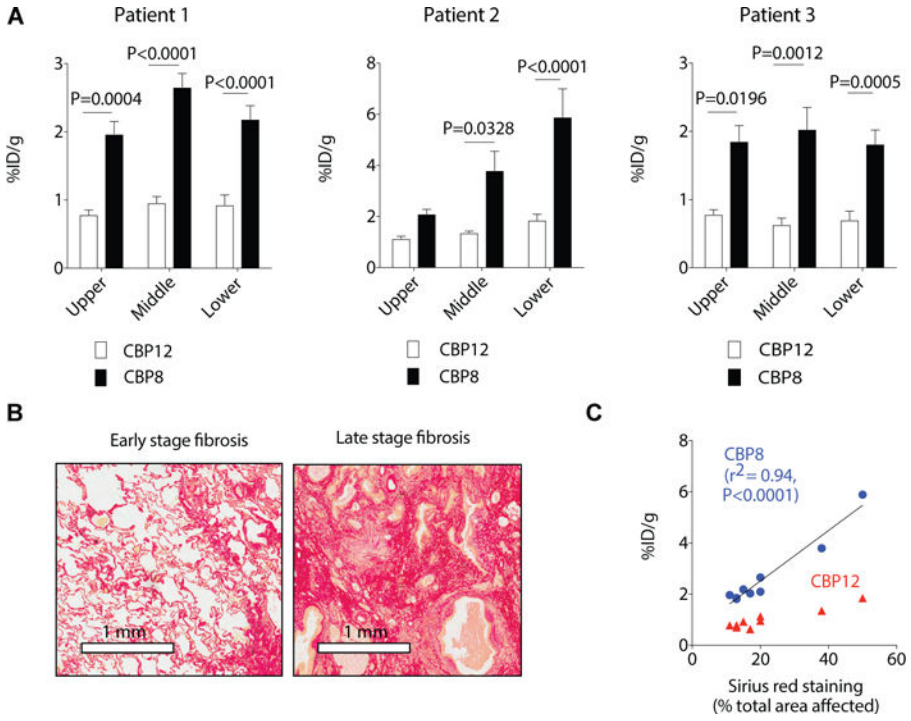

Fig. 5. Probe ^{68}Ga-CBP8 signal reflects changes in collagen concentration in human IPF lung tissues

A. Uptake of ^{68}Ga-CBP8 in human lung samples taken from the upper, middle, and lower lobes of explanted lung of IPF patients. The uptake is defined as %ID/g +/− standard error. Data were analyzed using one-way ANOVA, followed by post hoc Tukey tests with two-tailed distribution. For patient 1, n=5 (upper lobe), n=5 (middle lobe) and n=6 (lower lobe). For patient 2, n=8 (upper lobe), n=6 (middle lobe) and n=6 (lower lobe). For patient 3, n=5 (upper lobe), n=5 (middle lobe) and n=9 (lower lobe). **B.** Representative images of Sirius red staining of collagen showing early stage of IPF (left, lung section taken from the upper lobe of patient 2) characterized by thickening of the alveolar septa and knot-like formation and late stage of fibrosis (right, lung section taken from the lower lobe of patient 2) characterized by a denser deposition of collagen. **C**. Correlation of ^{68}Ga-CBP8 uptake in lung tissue samples from IPF patients with histological staining of collagen as measured by quantification of % collagen staining (Sirius red) in the area affected by disease (r^2=0.94, p<0.0001).